RESEARCH PAPER

Laser ablation-ICPMS analysis of trace elements in pyrite from the Tharsis massive sulphide deposit, Iberian Pyrite Belt (Spain)

Carmen Conde[1] · Fernando Tornos[2] · Leonid V. Danyushevsky[3] · Ross Large[3]

Abstract

High sensitivity laser ablation-inductively coupled plasma mass spectrometry (LA-ICPMS) has been utilized for the determination of trace elements in pyrite from the Tharsis VMS deposit, one of the most significant volcanogenic massive sulphide deposits in the southern Iberian Pyrite Belt. The study tracks the content and distribution of trace elements within the different facies of massive sulphides. Widespread and variable enrichment in elements such as Cu, Zn, and Pb in pyrite is interpreted to be due to the presence of nanoinclusions of chalcopyrite, sphalerite, and galena, respectively. A second group of elements, including As, Au, Tl, Mn and Mo, shows significant chemical variations according to the type of mineralization and the textural evolution of the pyrite. This behaviour is thought to be due to the fact that these metals are included in the mineral lattice and its incorporation is controlled by the degree of crystallinity, the temperature, and the redox conditions during crystallization. Early, spongiform and colloform pyrite in the stockwork is enriched in As and Au and interpreted to have formed from a high temperature and low fS_2–fO_2 fluid. Thallium, Mn, and Mo are enriched in pyrite precipitated at lower temperature and higher oxidation state, i.e., in the exhalative part of the system or in distal facies to the hydrothermal vents. In general, both Co and Ni show an irregular distribution and do not have the sympathetic distribution observed in equivalent studies.

Keywords LA-ICPMS · Pyrite · Trace elements · Tharsis · Massive sulphide · Iberian Pyrite Belt

Resumen

Este trabajo presenta los resultados del estudio del análisis de los elementos traza mediante la técnica de ablación láser con plasma de acoplamiento inductivo (LA-ICPMS) en pirita del yacimiento de Tharsis, uno de los mayores yacimientos de sulfuros masivos volcanogénicos de la parte sur del la Faja Pirítica Ibérica. El estudio determina el contenido y distribución de elementos traza en las diferentes facies de los sulfuros masivos. Se observa un generalizado y variable enriquecimiento en elementos como el Cu, Zn, y Pb en la pirita, interpretado como consecuencia de la presencia de nanoinclusiones de calcopirita, esfalerita y galena, respectivamente. Un segundo grupo de elementos como el As, Au, Tl, Mn y Mo muestran variaciones químicas significativas según el tipo de mineralización y la evolución textural de la pirita. Este comportamiento se debe a que la incorporación de estos metales en la red mineral está controlada por el grado de cristalinidad, temperatura y condiciones redox durante la cristalización. La pirita temprana, espongiforme y coloforme del stockwork, enriquecida en As y Au, se interpreta como formada a partir de un fluido de alta temperatura y bajo fS_2–fO_2. Tl, Mn y Mo están enriquecidos en pirita precipitada a una temperatura más baja y en un estado de oxidación más alto, es decir, en la parte exhalativa del sistema o en facies distales a los conductos hidrotermales. En general, tanto Co como Ni muestran una distribución irregular y no tienen la distribución observada en estudios equivalentes.

Palabras clave LA-ICPMS · pirita · elementos traza · Tharsis · sulfuros masivos · Faja Pirítica Ibérica

✉ Carmen Conde
carconri@gmail.com

1 Variscan GeoSciences Services. C/Vilar, Formoso 66, 37008 Salamanca, Spain

2 Instituto de Geociencias (CSIC-UCM), Dr Severo Ochoa, 7, 28040 Madrid, Spain

3 Centre for Ore Deposits and Earth Science, CODES, University of Tasmania, Hobart, TAS, Australia

1 Introduction

Pyrite is the most common mineral in volcanogenic massive sulphide (VMS) deposits worldwide (Franklin et al. 1981, 2005; Lydon 1988). This is especially relevant in the shale-hosted deposits of the southern Iberian Pyrite Belt (IPB), among which the giant Tharsis deposit (> 100 Mt) is one of the best examples. The deposit comprises several lensoidal sulphide bodies that are composed of > 95% fine-grained pyrite (Tornos et al. 1998).

Pyrite can host significant amounts of trace elements, both as mineral inclusions and as substitutions in its crystal structure, which can be detected and measured despite their low concentration levels by laser ablation inductively coupled plasma mass spectrometry (LA-ICPMS). The concentration and distribution of these elements may serve as a sensitive proxy for variations in the geochemical conditions that prevailed during sulphide precipitation. They can be also used in mineral exploration and in the development of genetic models for mineral deposits (Huston et al. 1995; Raymond 1996; Maier 2005; Yamaguchi and Ohmoto 2006; Large et al. 2009; Maslennikov et al. 2009; Koglin et al. 2010; Zhao et al. 2011).

In this paper, we present the first study of trace elements in pyrite from the Spanish sector of the IPB. Pyrite was analysed by LA-ICPMS combining a micro-solid laser ablation sampling system (LA) with a high sensitivity multi-element ICPMS. This is a modern microanalytical technique that yields much lower detection limits and much higher spatial resolution than electron microprobe (EPMA) (e.g., Cook et al. 2009a, b; Large et al. 2009; Koglin et al. 2010). LA-ICPMS technique is one of the most sensitive microbeam techniques for detecting ppm to ppb concentration (Sylvester 2008; Liu et al. 2013) becoming an excellent analytical tool in order to improve our understanding of pyrite composition, evolution and genesis.

Previous studies concerning mineralization from similar volcanogenic massive sulphide provinces and individual deposits such as Urals (Maslennikov et al. 2009); Kidd Creek (Canada) (Cabri et al. 1985) Queensland and Tasmania (Smith and Huston 1992; Huston et al. 1995; Raymond 1996), Bathurst Mining Camp (McClenaghan et al. 2004, 2009; Conde et al. 2008) and Neves Corvo, in the Portuguese sector of the Iberian Pyrite Belt (Serranti et al. 2002), have shown the importance of trace element distribution in pyrite, chalcopyrite and sphalerite as a geochemical tracer. This study provides the trace elements variations in pyrite from the different part of the orebody to improve and support the peculiar genesis of Tharsis volcanic-hosted massive sulphide.

2 Geological setting of the Tharsis massive sulphide

The Tharsis deposit (Filón Norte orebody), with original reserves of over 100 Mt at 0.5 Cu %, 0.6 Pb %, 2.7% Zn, 22 g/t Ag and 0.7 g/t Au (Tornos 2006), is one of the most important deposits in the Iberian Pyrite Belt. This metallogenic province, with more than 2,500 Mt, is considered as the major concentration of massive sulphide deposits in the world (Leistel et al. 1998; Tornos 2006). The deposit, located in the southern IPB (Fig. 1), is situated at the base of the Volcano-Sedimentary Complex (VS Complex) interbedded with shale and directly overlying the siliciclastic Phyllite-Quartzite (PQ) Group (shale and quartz sandstone). Particularly, the vs Complex in Tharsis is composed by a monotonous dark shale-rich sequence (Tharsis Fm.) tectonically overlain by mafic and felsic volcanic rocks (Tornos et al. 1998, 2008; Tornos and Conde 2002; Fig. 1b, c). There are no volcanic rocks interbedded with the massive sulphides, although laterally away from the deposit, the mineralized stratigraphic levels are marked by thin felsic volcaniclastic beds. Below the massive sulphides there is an irregular and thick feeder zone or stockwork, up to 200 m thick, hosted by a zone of chlorite-rich hydrothermal alteration that transgresses both the lowermost vs Complex and the PQ Group (Fig. 1c).

The Filón Norte massive sulphide (Fig. 2a) forms a thick lens (≈ 130 m) that is comprised of tectonically stacked units of what was originally a single large sheet-like massive sulphide body (ca. 20×4 km^2) (Tornos et al. 1998). In detail, the mineralization is made up of (Fig. 1d): (1) dominant monotonous *fine-grained pyrite* (< 400 μm) intergrown with minor amounts of chalcopyrite, sphalerite, galena, siderite, quartz, chlorite and other accessory minerals; (2) matrix-supported breccia with finely laminated pyrite, sphalerite and siderite in cm-sized angular fragments supported by coarse grained pyrite and siderite, occurring in the basal part of the deposit (*carbonate ore*) (Fig. 2b); (3) small and thin *conglomerate* beds that include clasts of massive sulphide and shale supported by fine-grained pyrite, that likely correspond to local debris flows potentially derived from the reworking of the carbonate ore (Fig. 2c); (4) the *laminated ore*, located in the uppermost part and in the contact with the hanging wall shale. It is made up of alternating shale and pyrite with abundant sedimentary structures (laminations, graded bedding, slumps, etc.) sometimes related to syn-sedimentary faults (Fig. 2d) and beneath siliceous shale alternating with white and grey chert (Fig. 2e); and, (5) the stockwork that consists in irregular veins composed by pyrite, minor quartz, Co–As–Fe–S minerals, and trace Bi–Pb–Cu–(Sb) sulphosalts, tellurides and native gold
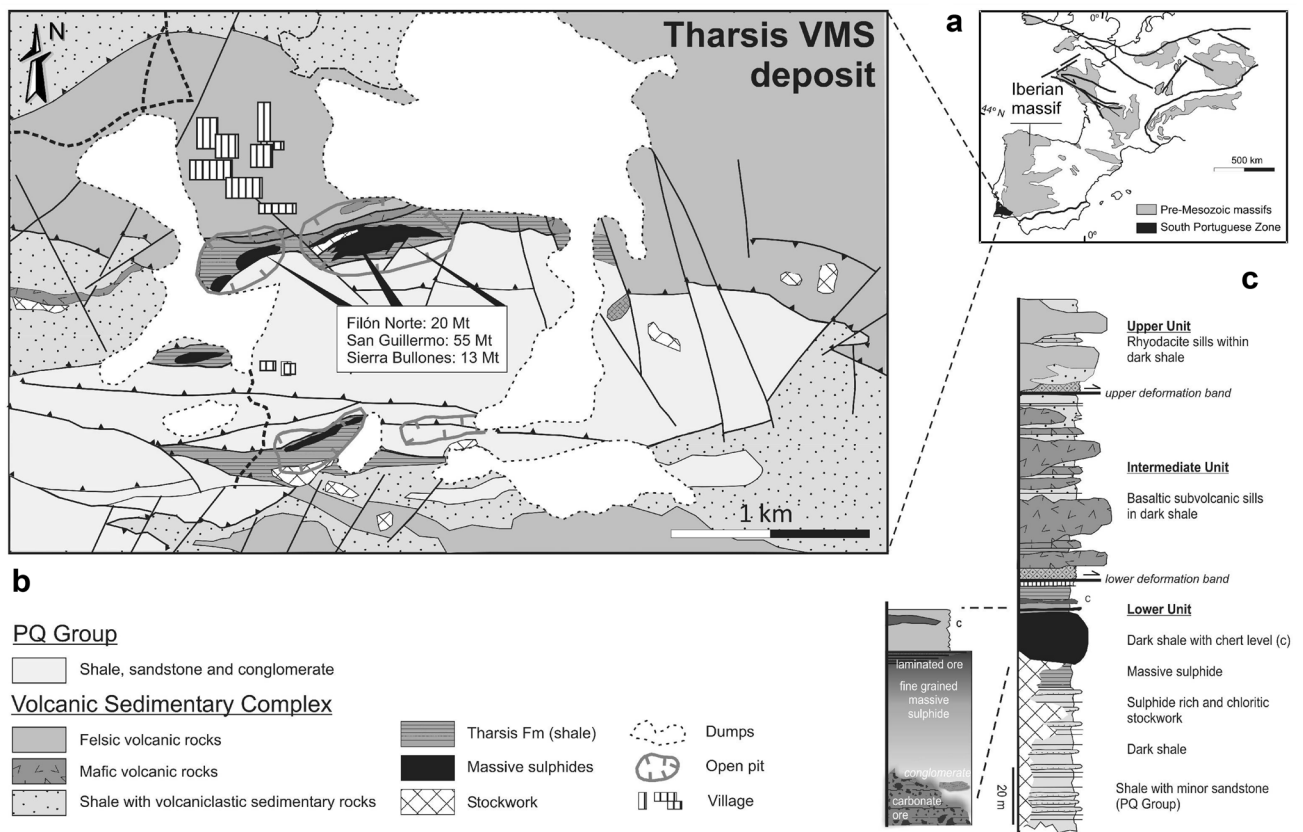
Fig. 1 Geological setting of the Tharsis deposit. **a** Schematic map of the Variscan Fold Belt in Europe (Oliveira and Quesada 1998). **b** Detailed geological map of the Tharsis area and location of the Filón Norte orebody (modified from Tornos et al. 2008). **c** General strati-graphic column of the Filón Norte orebody showing the distribution of the different types of mineralization (modified from Tornos and Conde 2002; Tornos et al. 2008)

(Fig. 2f) (Marcoux et al. 1996; Tornos et al. 1998) in chloritized shale.

The pyrite is of fine-grained, anhedral to subhedral shape (50–400 μm) with minor interstitial sulphides, siderite, quartz, chlorite, and other trace minerals (Marcoux et al. 1996; Tornos et al. 1998). It shows a range of different textures. The majority of the pyrite occurs as porous and subhedral textures. Also it is present as euhedral, spongiform, botryoidal, colloform, crustiform and laminated textures, but they are volumetrically minor.

Analytical methods The analysis of trace elements in pyrite was carried out on the LA-ICP MS facility at the CODES Ore Deposit Research Centre (Hobart, Australia). Trace elements were analysed via LA-ICPMS of spots 80 μm wide and 90 μm deep on pyrite grains larger than 150 μm. The total analytical run times were between 90 to 100 s, with background integration times of 30–35 s and 40–45 s for real ablation data or laser on (Fig. 3). Data were collected for 21 elements; ^{47}Ti, ^{51}V, ^{55}Mn, ^{57}Fe, ^{59}Co, ^{60}Ni, ^{65}Cu, ^{66}Zn, ^{75}As, ^{90}Zr, ^{95}Mo, ^{107}Ag, ^{111}Cd, ^{118}Sn, ^{121}Sb, ^{125}Te, ^{139}La, ^{197}Au,

^{205}Tl, ^{208}Pb and ^{209}Bi). The trace element composition of the internal standard STDGL-1 (a borate glass doped with powdered sulphide) was the primary calibration standard (Norman et al. 1998; Danyushevsky et al. 2003). Fe was used as an internal standard for the normalization of pyrite. The sulphur content was calculated using the theoretical stoichiometry or the empirical formula. In order to obtain the optimum results, the standard (STDGL-1) was analyzed twice every one and fifteenth analyses to account for the instrument drift, with a 80 μm beam and at 10 Hz.

Analyses were performed on 12 polished samples representing each of the principal ore facies. Within each sample, three to five pyrite grains were selected depending on the size and quality of the polishing; in each grain we performed three analyses. In total, 105 determinations were carried out. Analyzed samples includes 4 grains from the laminated ore, 11 from the main fine-grained massive sulphide ore, 4 from the conglomerate ore, 13 from the carbonate ore, and 7 from the footwall stockwork (Table 1).
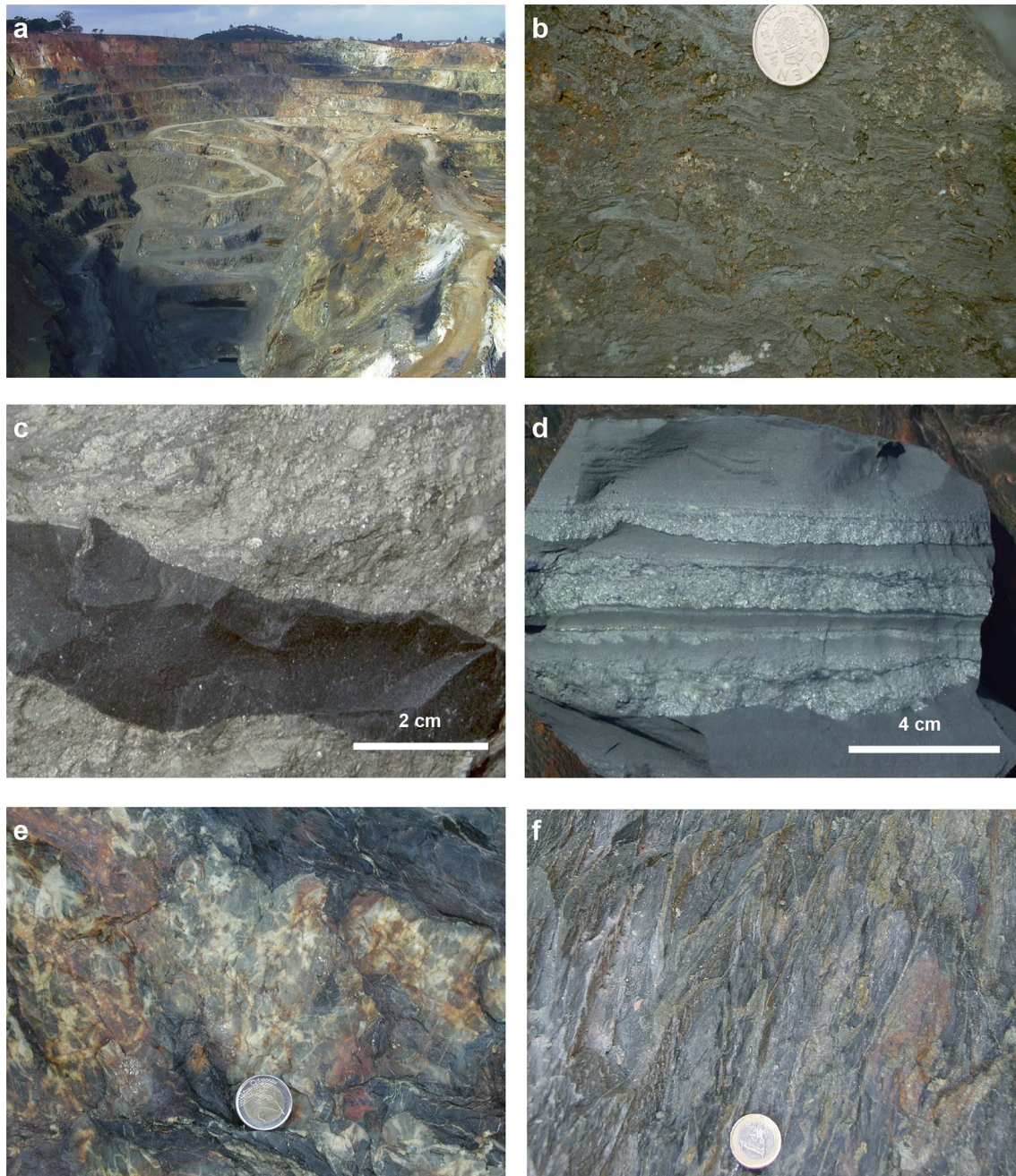
Fig. 2 Representative photographs from outcrops on the Filón Norte mineralization. **a** Overview of the Filón Norte open pit. **b** *Carbonate ore* showing fragments with fine alternating layers of siderite and sulphides (dominantly pyrite) cemented by coarse-grained pyrite and siderite (coin size, 2 cm). **c** Debris flow composed by unsorted fragments of massive sulphides and a large fragment of silicified shale supported by fine grained pyrite. **d** Representative sample of the *laminated ore* showing rhythmic layering. The lowermost part of the sequence includes a breccia with fragments of the carbonate ore overlain by finely layered pyrite with graded bedding and shale fragments. **e** Chert layer interbedded with silicified shale in the hanging wall of the massive sulphides (coin size, 2.5 cm). **f** Chloritized dark shale containing thin and irregular sulphide veins (stockwork) (coin size, 2.3 cm)

3 Results and discussion

Trace elements occur in pyrite in three modes: as inclusions and as stoichiometric and non-stoichiometric substitutions (Huston et al. 1995). Although visible inclusions exposed in the surface can be avoided, there always remains the possibility that the ablation pit intersects unobserved subsurface discrete nanoninclusions ($< 2–5$ μm). Therefore, the samples analyzed can show an inhomogeneity ablation profile even on the single-spot scale (< 100 μm).
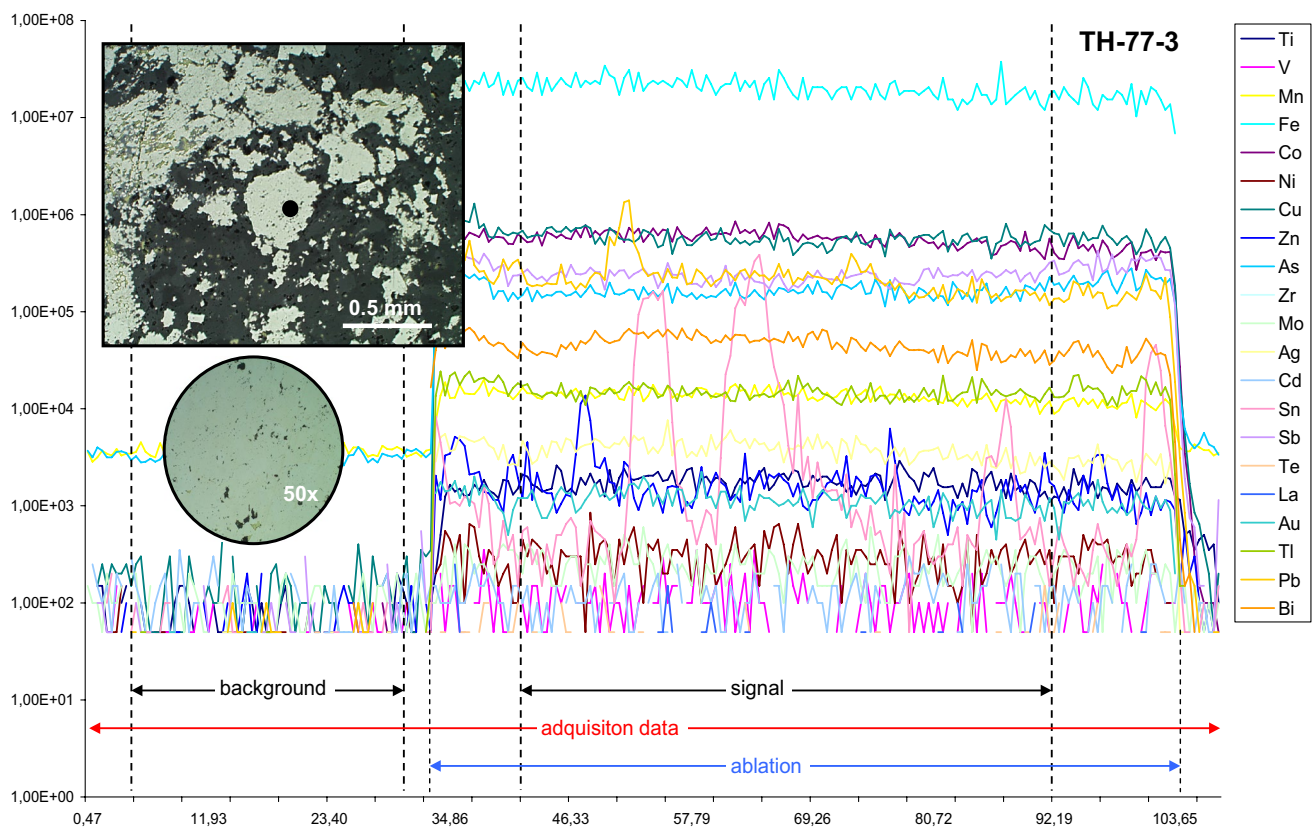
Fig. 3 Representative single-spot LA-ICPMS spectra of one analyzed pyrite, showing the data acquisition times and record for all elements analyzed. Times is represented in the X-coordinate (in seconds), and Y-axis shows the concentration of elements (weight)

Our results show that the contents of Cu, Pb and Zn in pyrite are erratic, but always high for all ore facies (Table 2). Concentrations summarized as histograms in Fig. 4 show high and variable concentrations in all the studied samples, with concentrations between 90 and 4900 ppm; highest contents are observed in pyrite from the laminated ore, particularly in Pb (up to 5000 ppm). However, all the analyzed pyrite grains show also high Cu (740–3230 ppm) and Zn (90–3790 ppm) contents. These concentrations are interpreted as reflecting the presence of nanometer-sized submicroscopic inclusions of galena and, to a lesser extent, of chalcopyrite and sphalerite in pyrite throughout the entire deposit (Fig. 5). The widespread presence of nanoinclusions of galena confirms that it was an early phase precipitating coevally with the earliermost pyrite. There seems to be a relationship between the concentrations in base metals and the pyrite texture. The highest Cu, Zn and Pb values, on average, occur in early pyrite with spongiform and framboidal morphology or as aggregates of fine-grained euhedral crystals. This early, low temperature pyrite probably formed during the maturation of intermediate sulphide compounds such on greigite or mackinawite and can host large amounts of metals in its disordered structure. In contrast, the Cu, Pb and Zn contents of individual and large euhedral crystals are never greater than 70 ppm. Presumably, the microinclusions have been taken out during later hydrothermal refining and coalesced in larger inclusions or individual grains (Large et al. 2009; McClenaghan et al. 2009). Also, it could be associated to the deposition of other sulphides in microcracks and dissolution patches in the post-kinematic stage (Marignac et al., 2003).

The correlation matrix between the analyzed elements shows that there is a strong general correlation between Pb and Ag in pyrite (r = 0.98, see Fig. 6a), except in the conglomerate facies wherein the Ag concentration is mainly positive correlated with Cu (Table 2). These relationships suggest that galena is the dominant carrier of silver in the whole deposit except in the conglomerate facies that is a Ag-rich fahlore (freibergite?). The laminated ore and the carbonate ore show a positive correlation between Pb and Bi (r > 0.9, Fig. 6b), possibly due to the presence of inclusions of Pb–Bi sulphosalts, such as wittichenite.

Arsenic is the most pronounced non-stoichiometric substitution in pyrite. The highest As concentrations occur in pyrite from the stockwork, but are also occasionally high in the conglomerate and the massive sulphide facies (Fig. 7). In the stockwork, the As content of pyrite ranges from 1650 to 4730 ppm (Table 1), among which the highest values are

Table 1 Summary of the concentrations of representative trace elements of pyrite grains from the different mineral types

	Ti (ppm)	V (ppm)	Mn (ppm)	Co (ppm)	Ni (ppm)	Cu (ppm)	Zn (ppm)	As (ppm)	Zr (ppm)	Mo (ppm)	Ag (ppm)	Cd (ppm)	Sn (ppm)	Sb (ppm)	La (ppm)	Au (ppm)	Tl (ppm)	Pb (ppm)	Bi (ppm)
Laminated ore **n=4**																			
Average	6.2	0.3	22.7	49.7	0.7	748.1	90.8	517.0	<0.1	0.8	15.7	0.3	13.2	219.5	<0.01	0.6	148.5	4945.3	93.8
max	7.0	0.9	39.1	95.6	0.9	1447.3	227.3	1003.0	<0.1	1.9	35.6	0.5	23.8	315.0	<0.1	0.8	512.2	13,744.2	179.5
min	4.8	<0.1	4.4	2.2	0.4	160.2	19.4	105.0	<0.01	0.2	6.1	0.1	0.5	182.6	<0.01	0.5	3.9	1683.0	45.7
SD	1.0	0.4	14.4	38.8	0.2	603.4	95.7	369.1	–	0.8	13.5	0.2	11.5	63.8	–	0.1	244.6	5871.1	59.5
>MDL (%)	100	100	100	100	100	100	100	100	100	100	100	75	100	100	100	100	100	100	100
Fine grained ms **n=11**																			
Average	8.4	0.4	26.3	62.6	5.2	1065.0	554.0	565.3	<0.1	0.6	22.1	1.5	13.9	481.5	<0.01	1.5	25.6	3576.8	184.9
max	12.7	1.4	160.3	158.8	17.2	2647.0	4644.9	2258.3	<0.1	3.2	116.0	10.1	94.6	1975.6	<0.1	6.3	107.0	12,846.3	1453.1
min	6.2	<0.1	4.3	0.2	0.3	55.1	1.4	6.5	<0.1	<0.1	0.1	0.2	0.2	1.8	<0.01	<0.1	<0.1	4.1	0.5
SD	1.7	0.4	46.5	52.5	5.6	947.8	1371.8	658.0	–	0.9	38.4	2.9	27.1	609.6	–	1.9	43.6	3921.9	424.6
>MDL (%)	100	100	100	100	100	100	100	100	36	82	100	73	100	100	82	91	100	100	100
Conglomerate **n=4**																			
Average	8.6	1.6	362.1	396.1	2.1	3222.2	852.1	1433.7	<0.1	0.3	10.0	1.8	6.0	209.5	<0.1	3.5	0.3	2385.9	91.6
max	9.7	4.9	829.8	734.3	3.1	6570.5	1441.7	4811.5	<0.1	0.5	16.5	2.7	10.1	308.6	<0.1	6.5	0.8	4409.4	158.1
min	7.5	<0.1	4.4	157.4	1.3	1.6	1.1	221.9	<0.1	0.1	0.1	0.2	0.2	3.1	<0.01	<0.1	<0.1	6.9	0.2
SD	0.9	2.2	355.9	252.8	0.8	2692.8	608.1	2253.4	–	0.2	7.1	1.1	4.3	142.6	–	2.6	0.3	2170.7	66.2
>MDL (%)	100	100	100	100	100	100	100	100	75	100	100	100	100	100	75	100	100	100	100
Carbonate ore **n=13**																			
Average	11.0	2.6	308.1	93.5	7.8	1759.7	3785.6	747.8	0.1	2.2	20.5	8.3	38.7	384.8	<0.1	2.2	32.2	3467.3	58.8
max	43.7	11.9	1348.4	260.5	40.2	4888.8	18,297.0	3131.0	1.4	19.2	113.5	39.3	134.2	753.3	<0.1	8.2	376.8	25,215.5	282.5
min	6.6	<0.1	4.5	3.3	0.5	192.9	7.2	277.4	<0.1	0.1	3.9	0.1	1.8	71.5	<0.01	0.2	0.3	133.9	19.4
SD	9.9	3.4	367.0	89.0	10.8	1472.7	5533.5	761.7	0.4	5.2	29.4	12.2	41.6	203.8	–	2.4	103.6	6630.9	69.7
>MDL (%)	100	100	100	100	100	100	100	100	77	85	100	85	100	100	85	100	100	100	100
Stockwork **n=7**																			
Average	31.8	5.3	67.4	121.1	34.7	941.0	142.2	2533.2	0.5	0.3	4.9	0.4	13.7	161.0	0.4	3.5	51.7	1307.1	84.6
max	173.2	35.4	423.8	337.1	86.8	2143.0	698.5	4732.3	3.4	1.2	7.8	1.0	48.1	263.6	2.6	8.0	175.6	5351.6	257.3
min	5.2	<0.1	2.1	8.4	0.7	185.7	3.5	1656.6	<0.01	0.1	0.3	0.2	0.2	5.3	<0.01	1.2	<0.1	5.4	6.8
SD	62.4	13.3	157.3	132.2	38.0	827.1	251.8	1223.7	1.3	0.4	2.9	0.3	19.8	101.0	1.0	2.4	81.4	1963.4	92.0
>MDL (%)	100	100	100	100	100	100	100	100	57	100	100	71	100	100	29	100	100	100	100

The italicized values correspond to the values very low

Analysis by LA-ICP MS; concentration in ppm

n number of selected samples, *max.* maximum, *min.* minimum, *SD* standard deviation, *>MDL(%)* percentage of analyses above the minimum detection limit

Table 2 Summary of the correlation coefficients for selected trace elements in pyrite (Pearson's R)

Ore type	Samples	Ag&Pb	Ag&Cu	Pb&Bi	As&Au	Bi&Au	Co&Au	Co&Ni	Sn&Cu	Sn&Zn
Total	41									
Banded ore	4	***0.98***	0.35	***0.95***	0.64	− 0.18	− 0.79	***0.92***	0.44	− 0.60
Fine-grained ms	11	***0.90***	0.44	0.40	− 0.12	0.80	0.02	0.31	0.58	***0.98***
Conglomerate	4	0.47	***0.98***	0.41	0.76	***0.99***	0.38	0.72	***0.90***	***0.94***
Carbonate ore	13	***0.95***	− 0.32	***0.97***	0.89	− 0.03	− 0.22	0.01	0.31	− 0.09
Stockwork	7	0.61	0.66	-0.39	− 0.14	***0.94***	0.73	0.42	0.78	0.63

Bold and italicized values indicate the higher values and with a posite correlation
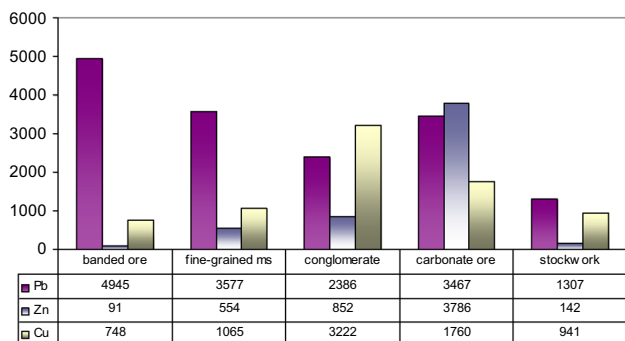
Fig. 4 Histograms showing the Cu, Pb and Zn concentrations in pyrite of the mineral types from Filón Norte massive sulphide deposit. Dataset table shows a summary of Cu, Pb and Zn concentration (on average) in ppm for all types of pyrite

recorded from the framboidal and colloform pyrite. Similar studies in other VMS deposits have shown that arsenic to have a good correlation with gold and other trace elements (e.g., Cook and Chryssoulis 1990; McClenaghan et al. 2004, 2009; Large et al. 2009). Here, the gold content of pyrite ranges from 1 to 8 ppm (Table 1). Data from pyrite of the laminated ore, conglomerate and carbonate ore show a positive correlation between As and Au (Fig. 6c, see Table 2); in contrast, they show a negative correlation in pyrite from the fine-grained massive sulphide and the stockwork. Positive correlation is typical in the As-rich pyrite of the massive sulphides in the Iberian Pyrite Belt. The relationship between As enrichment and Au in pyrite is probably due to supersaturation of early pyrite formed at relatively low sulphur fugacities at high (> 250 °C) temperatures. Rapid precipitation of pyrite leads to both the colloform texture and to the incorporation of As and Au in the nascent pyrite lattice. The As substitution for S^{2-} in the pyrite structure within sulphur-deficient conditions forms arsenical pyrite that is a metastable solid solution $Fe(As,S)_2$ (Huston et al. 1995). Regarding the negative correlation between As and Au, some authors suggest that it could be due to the presence of nanoinclusions of Au-bearing tellurides which are more stable than hypothetical As–Au phases (Maslennikov et al. 2009). Tellurides are not described in the massive sulphide mineralization at Tharsis but both As- and Te-bearing minerals are common in the stockwork in the form of arsenopyrite and Co-As minerals as cobaltite (CoAsS) and glaucodot
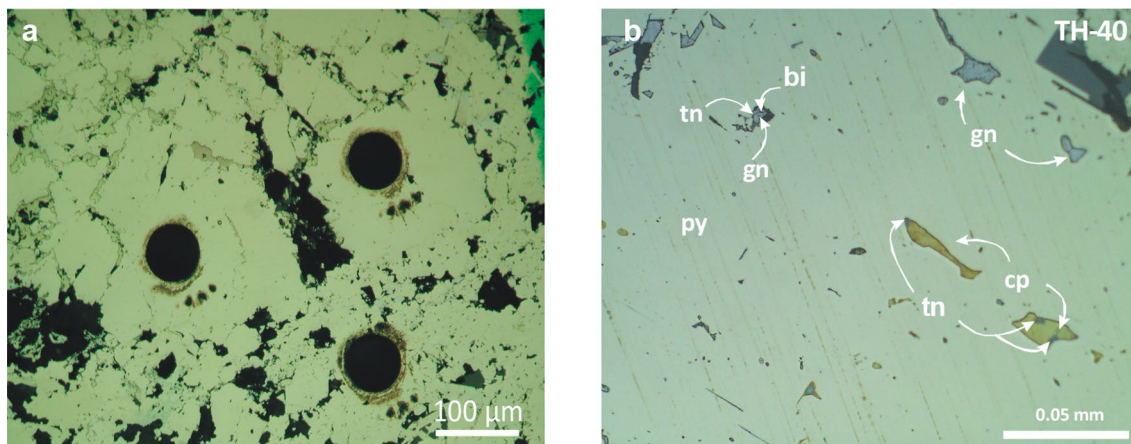

Fig. 5 Reflected-light photomicrographs of pyrite from Filón Norte. **a** Example of subhedral pyrite ablated for analysis. **b** Subhedral pyrite showing microinclusions of galena, chalcopyrite, Pb-Bi sulphosalts, bismuth and tennantite-tetrahedrite (TH-40: carbonate ore). (Mineral abbreviations from: https://www.unige.ch/sciences/terre/research/Groups/mineral_resources/opaques/ore_abbreviations.php)
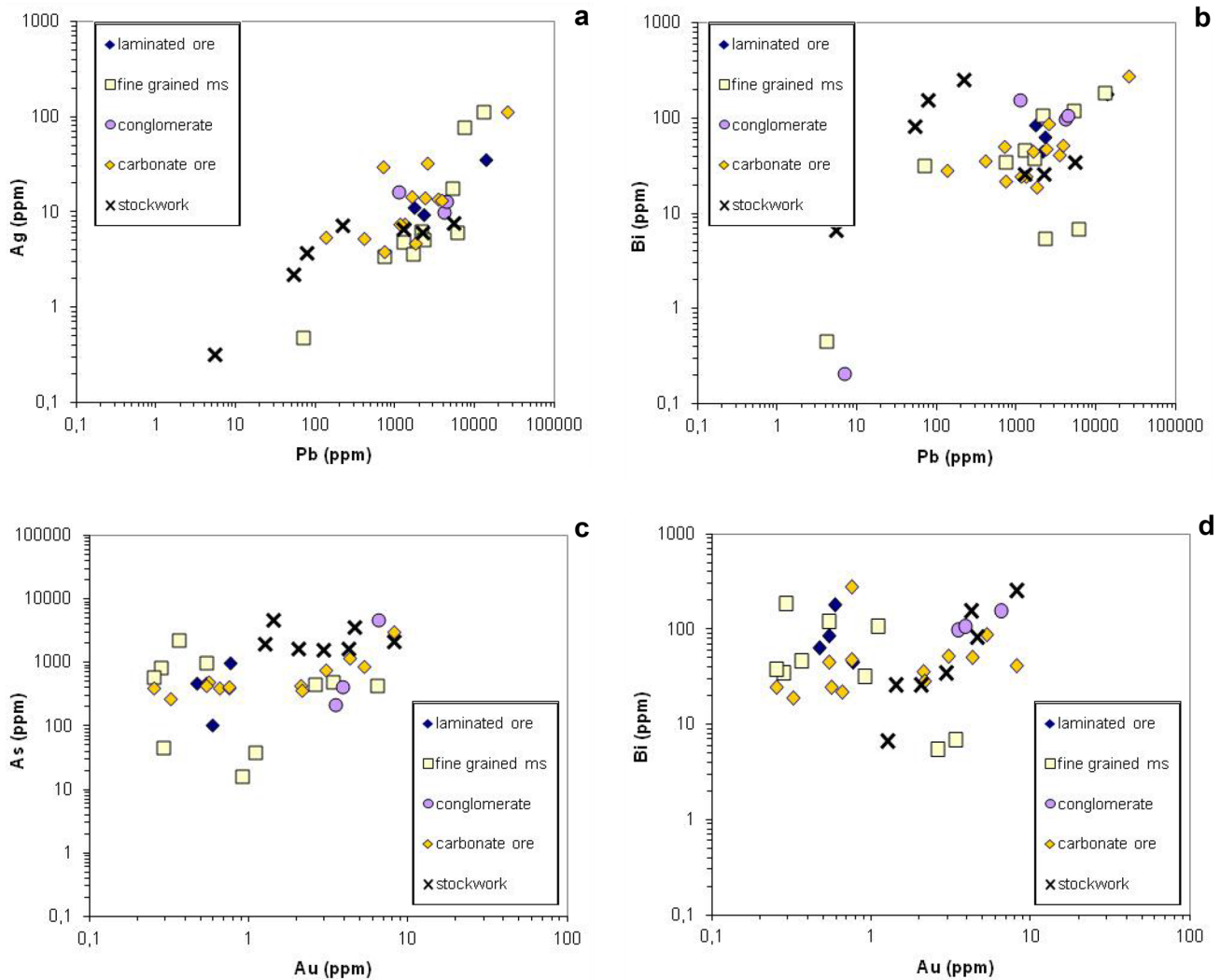
Fig. 6 Binary plots of selected trace elements in pyrite. **a** Ag vs. Pb diagram showing a positive correlation trend, mainly in pyrite from laminated ore, carbonate ore and fine-grained massive sulphide (r > 0.90). **b** Plot of Bi vs. Pb displaying a correlation index higher than r = 0.95 in the laminated and carbonate ore. **c** As vs. Au diagram showing the positive correlation in pyrite from conglomerate, carbonate and laminated ore. **d** Bi vs. Au discrimination plot showing the clear positive correlation of pyrite from stockwork

([Co, Fe]AsS), and joseite ($Bi_4(S,Te)_3$), respectively (Marcoux et al. 1996; Tornos et al. 1998). The fine-grained massive sulphide and the stockwork also show positive Bi-Au and Co-Au correlations (Fig. 6d, see Table 2). In this case, data are consistent with the presence of cobalt-bearing minerals (e.g., cobaltite, alloclasite and/or glaucodot) and Bi minerals (kobellite and/or bismuthinite), especially in the stockwork (Marcoux et al. 1996; Tornos et al. 1998). This confirms that Au can be associated with Bi-bearing sulphides and the fact that in the stockwork gold always occurs as inclusions in cobaltite-glaucodot (Tornos et al., 1998). The conglomerate facies shows a good relationship between Bi and Au (r = 0.99).

Since there is no record of thallium-bearing minerals in the IPB, it is likely that thallium is incorporated to the pyrite lattice, having concentrations between 0.01 and 512 ppm. Again, the highest contents are associated with framboidal or colloform pyrite (> 100 ppm); however, the most significant enrichment (> 500 ppm) was found in the euhedral and sub-euhedral pyrite from the laminated ore (Fig. 7). The presence of Tl in pyrite is commonly product of the substitution of Fe^{3+} for Tl^{3+} in the As-rich pyrite (Cook and Chryssoulis 1990), something supported by the also positive correlation between Tl and As in the carbonate ore (r = 0.94). However, the Tl enrichment related to colloform pyrite shows an apparent positive correlation with Pb (r = 0.10). In this case, the presence of Tl could be due to the presence of galena micro-inclusions, which under conditions of low temperature can show significant substitution of $2Tl^+$ for Pb^{2+} (Maslennikov et al. 2009).
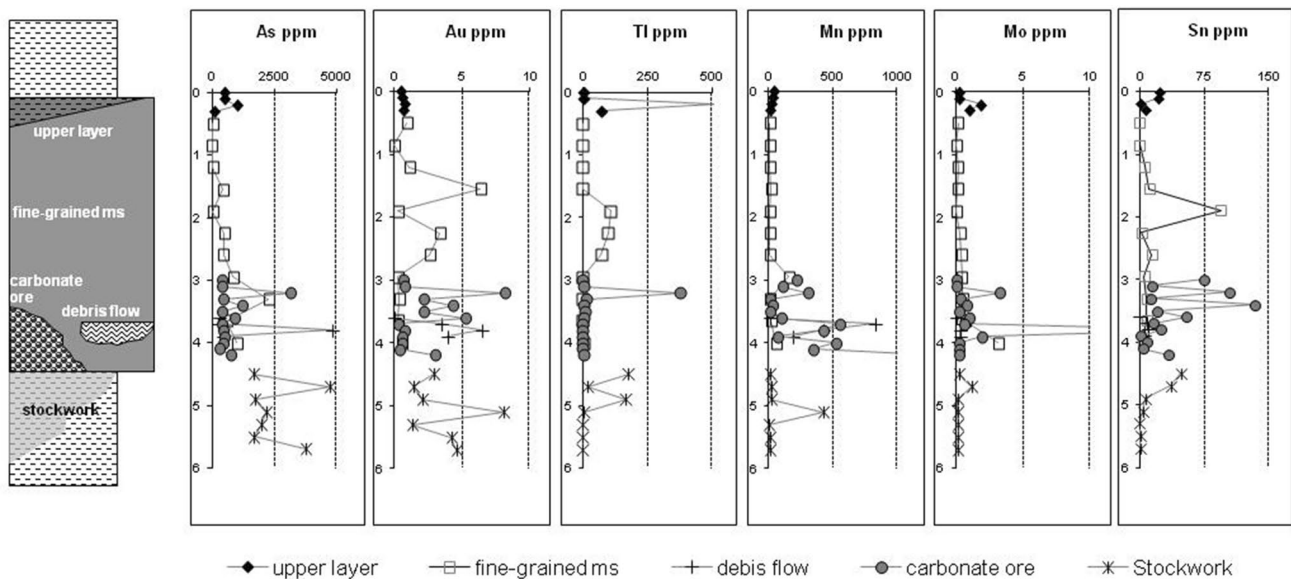
Fig. 7 Section of the Filón Norte orebody (Tharsis) showing the distribution of selected trace elements in pyrite from the different mineralization types (in ppm)

The concentration of Mn ranges between tens to a few hundred ppm (Table 1). The Mn concentration is highest in the finely laminated pyrite from the carbonate ore and can be occasionally high in the conglomerate, with average concentrations of > 300 ppm and 360 ppm, respectively (Fig. 7). In some cases it could be interpreted to presence of Mn-bearing carbonate inclusions—especially in the carbonate ore. In the conglomerate, textures and geochemical data support that the enrichment in Mn is due to simple cation exchange between the Fe^{2+} by Mn^{2+} which could be enhanced by the low temperature of precipitation and, especially, to a less reduced state of the environment of precipitation.

Generally, the pyrite of the carbonate ore is enriched in Mo (avg. 2.2 ppm) with respect to the other facies (0.3–0.8 ppm). The incorporation of small amounts of Mo in the structure of pyrite is thought also to be related to the redox conditions, with Mo enrichment under locally oxidizing conditions—potentially related to CO_2 production during coupled sulfate reduction—organic matter oxidation—or late hydrothermal recrystallization (Huston et al. 1995). Also, the increasing Mo concentration in the pyrite can be a result of the influx in the distal facies of unmodified seawater carrying MoO_4^{2-}. Here, more oxidizing conditions facilitate the incorporation of Mo into the pyrite structure (Mukherjee and Large 2017).

The Ti content is broadly uniform in all ore facies, and exhibits concentrations from 6 to 11 ppm. One analysis from the stockwork zone yielded a highly anomalous value of 170 ppm, which is likely due to record ablation of a rutile or ilmenite inclusion.

In general, the massive sulphide deposits of the Iberian Pyrite Belt have more Sn than other massive sulphide deposits elsewhere (Solomon et al. 2002). This is especially noticeable in the Neves Corvo deposit (Portugal) where the massive sulphides contain average contents of 2.2% Sn and include local zones of high grade to massive cassiterite (> 8% Sn) (Relvas 2000; Serranti et al. 2002). In Tharsis, all of our analyses record measureable Sn, with an average concentration of 13 ppm Sn, but there is an anomalous enrichment of up to 130 ppm in pyrite of the carbonate ore (Table 1). Stannite has been described previously as an accessory mineral at Tharsis (Tornos et al. 1998), but our results indicate that there is not always a good correlation between Cu and Sn within the pyrite (Table 2). Thus, stannite cannot be the sole, and perhaps not even the principal, Sn-bearing phase in the pyrite. Alternatively, the Sn budget may be accounted by Sn held in solid solution in pyrite as has been suggested by Cabri et al. (1985) for the elevated Sn content in massive sulphides at Kidd Creek. This could be possible at Tharsis, but petrography indicates that the high Sn contents are largely due to the presence of SnO_2 (cassiterite) inclusions in sphalerite, which coprecipitated with pyrite at intermediate fS_2 values (Tornos et al. 1998). Thus, is likely that the high Sn contents are due to the presence of nanoinclusions of cassiterite in pyrite.

Co and Ni are the most common trace elements in pyrite, and are the elements that have been most widely investigated as possible tracers of the origin and conditions of precipitation of the pyrite (Walshe and Solomon 1981; Roberts 1982; Brill 1989; Huston et al. 1995; Raymond 1996; Clark et al. 2004; Koglin et al. 2010). In some cases, the Co:Ni ratio has
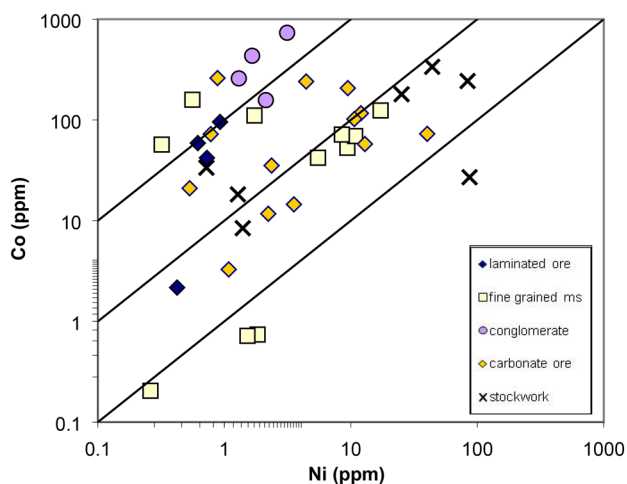
Fig. 8 Binary plot of Co vs. Ni content showing the distribution of Co/Ni ratios of pyrite

been employed to discriminate the environment of formation (Hawley and Nichol 1961; Bajwah et al. 1987), although the robustness of this classification has also been questioned (Campbell and Ethier 1984). Both Co and Ni usually occur as stoichiometric substitutions in pyrite, wherein they substitute the Fe lattice sites since they are isomorphous and chalcophile (Springer et al. 1964). The petrogenetic interpretation of the Co and Ni contents in pyrite has been discussed by Bralia et al. (1979), Brill (1989) and Bajwah et al. (1987), which propose diagrams showing the relationship between these contents and the style of mineralization.

At Tharsis, the highest concentrations of Co (avg. 120 ppm) occur in the footwall stockwork zone and in the conglomerate facies (avg. 360 ppm). In both ore facies, the highest values are in the aggregates of fine pyrite crystals and porous pyrite. Pyrite in the laminated ore contains the lowest average Co (<50 ppm). Ni contents are systematically lower than Co concentrations. Pyrite in most of the ore facies contains less than 8 ppm Ni, except in the footwall stockwork where Ni concentrations exceed 85 ppm (Table 1). Enrichment of Co and Ni in pyrite is here likely attributable to the higher temperatures (125-240 ℃) and lower fS_2 conditions of the stockwork zone, that favour the replacement of Fe by Co in the lattice. As quoted above, cobaltite and other Co-bearing phases are ubiquitous in the stockwork mineral assemblage (Tornos et al. 1998).

Based on Brill (1989) diagram the pyrite at Tharsis shows variable Co:Ni values that plot from the sedimentary (< Co/Ni = 1) to the volcano-exhalative fields (> Co/Ni = 10), confirming that these diagrams are not able to discriminate between ore-forming environments (Fig. 8). In fact, these models do not take into account multiple variables including if the system is undersaturated or supersaturated in both Co

and Ni. That is, only when pyrite coexists with Ni- and Co-rich phases then the Ni and Co contents in pyrite depend on its capability to accept them in the lattice. In undersaturated systems the situation is more complex and controlled by the $K_D^{pyrite-fluid}$ and their concentrations in the fluid. Since cobaltite is the only discrete Co-rich phase at the Tharsis stockwork and is only locally present, it is unlikely that Co and Ni can be used as petrogenetic indicators here.

4 Conclusions

The detailed geochemical study of pyrite from the Tharsis massive sulphide deposit shows the existence of a systematic enrichment in some trace elements. The results show a coherent distribution according to the texture and type of mineralization. The anomalously high concentrations of Cu, Pb, Zn, Ag, Sn and Ti are interpreted to be due to the presence of nanoinclusions of minerals that are also present as discrete grains within the deposit product of later hydrothermal refining or metamorphism. The concentration of As, Mn, Mo, Tl, Ni, Co and Au is more irregular and probably reflect the incorporation in the pyrite lattice. This was probably controlled by the temperature of the fluid, fO_2-fS_2 conditions and the degree of crystallinity of the host pyrite mineral. Whereas Mo, Mn and Tl are enriched in the apparently more oxidized and cooler distal zones, As, Co and Au concentrate preferentially in the proximal, hotter and low-fS_2 environments. In general, early pyrite precipitated at lower temperatures and showing lower crystal ordering—probably due to rapid precipitation induced by supersaturation or microbial precipitation- has higher concentrations of these metals; major enrichment occurs in pyrite with the most primitive textures (framboidal and colloform) but there is a strong depletion in the more mature euhedral pyrite. An evolution from an early, high temperature, reduced and sulphur-poor system, represented by the stockwork, to a S_2-rich, oxidized and cooler environment in the massive sulphides is consistent with the contents of most lattice-related elements.

These results demonstrate that the trace elements concentration in the pyrite could be of help to define a strategic signature in the mining exploration. The chemical variation would allow distinguishing the proximal and distal zone of the volcanic massive sulphides, as stockwork zones and late remobilizations veins, because the trace elements precipitation is determined function of specific physicochemical and redox conditions.

Compliance with ethical standards

Conflicts of interest/Competing interest The authors declare no conflict of interest.

Availability of data and material See Online Appendix.

References

Bajwah, Z. U., Seccombe, P. K., & Offer, R. (1987). Trace element distribution Co: Ni ratios and genesis of the Big Cadia iron-copper deposit, New South Wales, Australia. *Mineralium Deposita, 22,* 292–300.

Bralia, A., Sabatini, G., & Troja, F. (1979). A revaluation of the Co/Ni ratio in pyrite as geochemical tool in ore genesis problems. *Mineralium Deposita, 14,* 353–374.

Brill, B. (1989). Trace-element contents and partitioning of elements in ore minerals from the CSA Cu-Pb-Zn deposit, Australia. *The Canadian Mineralogist, 27,* 263–274.

Cabri, L. J., Campbell, J. L., Laflamme, J. H. G., Leigh, R. C., Maxwell, J. A., & Scott, J. D. (1985). Proton-microprobe analysis of trace elements in sulfides from some massive-sulfide deposits. *The Canadian Mineralogist, 23,* 133–148.

Campbell, F. A., & Ethier, V. G. (1984). Nickel and cobalt in pyrrhotite and pyrite from the Faro and Sullivan orebodies. *The Canadian Mineralogist, 22,* 503–506.

Clark, C., Grguric, B., & Schmidt Mumm, A. (2004). Genetic implications of pyrite chemistry from the Palaeoproterozoic Olary Domain and overlying Neoproterozoic Adelaidean sequences, northeastern South Austrlia. *Ore Geology Reviews, 25,* 237–257.

Conde, C.,, Lentz, D. R., Walker, J.., Huard, A., Tornos, F. (2008). Petrology and geochemistry of the Cu-rich zone at the Brunswick No. 6 Zn-Pb-Cu-Ag VMS deposit, Bathurst Mining Camp, New Brunswick (Canada). In: 33rd International Geological Congress, Oslo.

Cook, N. J., & Chryssoulis, S. L. (1990). Concentrations of invisible gold in the common sulfides. *The Canadian Mineralogist, 28,* 1–16.

Cook, N. J., Ciobanu, C. L., & Mao, J. W. (2009a). Textural control on gold distribution in As-free pyrite from the Dongping, Huangtuliang and Hougou gold deposits, North China Craton, (Hebei Province, China). *Chemical Geology, 204,* 101–121.

Cook, N. J., Ciobanu, C. L., Pring, A., Skinner, W., Shimizu, M., Danyushevsky, L., et al. (2009b). Trace and minor elements in sphalerite: A LA-ICPMS study. *Geochimica et Cosmochimica Acta, 73,* 4761–4791.

Danyushevsky, L. V., Robinson, P., McGoldrick, P., Large, R. R., Gilbert, S. (2003). LA-ICPM of sulfides: evaluation of an XRF glass disc standard for analysis of different sulphide matrixes. In: *2003 Goldschmidt Conference, Japan.* Geochemica Cosmochimica Acta 67, p A73

Franklin, J. M., Gibson, H. L., Galley, A. G., Jonasson, I. R. (2005). Volcanogenic massive sulfide deposits. In: Hedenquist, J. W., Thompson, J. F. H., Goldfarb, R. J., Richards, J. P. (eds.) *Economic geology 100th anniversary volume* (pp 523–560). Society of Economic Geologist.

Franklin, J. M., Sangster, D. M., Lydon, J. W. (1981). Volcanic-associated massive sulphide deposits. In: Skinner, B. J. (Ed) *Economic geology seventy-fifth anniversary volume* (pp 485–627). Society of Economic Geologists.

Hawley, J. E., & Nichol, I. (1961). Trace elements in pyrite, pyrrhotite and chalcopyrite of different ores. *Economic Geology, 56,* 467–487.

Huston, D. L., Sie, S. H., Suter, G. F., Cooke, D. R., & Both, R. A. (1995). Trace elements in sulfide minerals from eastern Australia volcanic-hosted massive sulphide deposit. *Economic Geology, 90,* 1167–1196.

Koglin, N., Frimmel, H. E., Lawrie, W. E., & Brätz, H. (2010). Trace-element characteristics of different pyrite types in Mesoarchaean to Palaeoproterozoic placer deposits. *Mineralium Deposita, 45,* 259–280.

Large, R. R., Danyushevsky, L., Hollit, C., Maslennikov, V., Meffre, S., Gilbert, S., et al. (2009). Gold and trace element zonation in pyrite using a laser imaging technique: implications for the timing of gold in orogenic and Carlin-style sediment-hosted deposits. *Economic Geology, 104,* 635–668.

Leistel, J. M., Marcoux, E., Thieblemont, D., Quesada, C., Sanchez, A., Almodóvar, G. R., et al. (1998). The volcanic-hosted massive sulphide deposits of the Iberian Pyrite Belt: Review and preface to the special issue. *Mineralium Deposita, 33,* 2–30.

Liu, Y., Hu, Z., Li, M., & Gao, S. (2013). Applications of LA-ICP-MS in the elemental analyses of geological samples. *Chinese Science Bulletin, 58,* 3863–3878.

Lydon, J. W. (1988). Volcanogenic massive sulphide deposits, part 1, A descriptive model. In: Roberts, R. G., Sheahan, P. A .(eds.) *Ore deposit models. Geoscience Canada,* Rep. Ser. 3. St. John's, Newfoundland, pp. 45–153

Maier, R. C. (2005). Pyrite trace element halos to northern Australian sediment-hosted Zn-Pb-Ag deposits. In: Mao J, Bierlein FP (ed) Mineral deposit research: meeting the global challenge (pp 18–20). Proceedings of the Eighth Biennial SGA Meeting, China

Marcoux, E., Moelo, Y., & Leistel, J. M. (1996). Bismuth and cobalt minerals: indicators of stringer zones to massive-sulfide deposits, South Iberian Pyrite Belt. *Mineralium Deposita, 31,* 1–26.

Marignac, C., Diagana, B., Cathelineau, M., Boiron, M. C., Banks, D., Fourcade, S., & Vallance, J. (2003). Remobilisation of base metals and gold by Variscan metamorphic fluids in the soutyh Iberian pyrite belt: evidence from the Tharsis VMS deposit. *Chemical Geology, 194,* 143–165.

Maslennikov, V. V., Maslennikova, S. P., Large, R. R., & Danyushevsky, L. V. (2009). Study of trace element zonation in vent chimneys from the Silurian Yaman-Kasy volcanic-hosted massive sulphide deposit (southern Urals, Russia) using Laser

Ablaiton-Inductively Coupled Plasma Mass Spectrometry (LA-ICPMS). *Economic Geology, 104,* 1111–1141.

McClenaghan, S. H., Lentz, D. R., & Cabri, L. J. (2004). Abundance and speciation of gold in massive sulphides of the Bathurst Mining Camp, New Brunswick, Canada. *The Canadian Mineralogist, 42,* 851–871.

McClenaghan, S. H., Lentz, D. R., Martin, J., & Diegor, W. G. (2009). Gold in the Brunswick No. 12 volcanogenic massive sulphide deposit, Bathurst Mining Camp, Canada: Evidence from bulk ore analysis and laser ablation ICP-MS data on sulphide phases. *Mineralium Deposita, 44,* 523–557.

Mukherjee, I., & Large, R. (2017). Application of pyrite trace element chemistry to exploration for SEDEX style Zn-Pb deposits: McArthur Basin, Northern Territory, Australia. *Ore Geology Reviews, 81,* 1249–1270.

Norman, M. D., Griffin, W. L., Pearson, N. J., García, M. O., & O'Reilly, S. Y. (1998). Quantitative analysis of trace element abundances in glasses and minerals: a comparison of laser ablation inductively coupled plasma mass spectrometry, solution inductively coupled plasma mass spectrometry, proton microprobe and electron microprobe data. *Journal of Analytical Atomic Spectrometry, 13,* 477–483.

Oliveira, J.T., & Quesada, C. (1998). A Comparison of Stratigraphy, Structure and Paleogeography of the South Portuguese Zone and Southwest England. European Variscides Geoscience in southwest England, The Scott Simpson Lecture, Annual Conference of the Ussher Society, pp. 141–159.

Raymond, O. L. (1996). Pyrite composition and ore genesis in the Prince Lyell copper deposit, Mt Lyell mineral field, western Tasmania, Australia. *Ore Geology Reviews, 10,* 231–250.

Relvas, J. M. R. S. (2000). Geology and metallogenesis at the Neves Corvo deposit, Portugal. Ph.D. thesis, Universidade de Lisboa, 319 pp.

Roberts, F. I. (1982). Trace element chemistry of pyrite: a useful guide to the occurrence of sulphide base metal mineralization. *Journal of Geochemical Exploration, 17,* 49–62.

Serranti, S., Ferreini, V., Masi, U., & Cabri, L. J. (2002). Trace-element distribution in cassiterite and sulfides from rubané and massive ores of the Corvo deposit, Portugal. *The Canadian Mineralogist, 40,* 815–835.

Smith, R. N., & Huston, D. L. (1992). Distribution and association of selected trace elements at the Rosebery deposit, Tasmania. *Economic Geology, 87,* 706–719.

Solomon, M., Tornos, F., & Garpas, O. C. (2002). Explanation for many of the unusual features of the massive sulphide deposit of the Iberian pyrite belt. *Geology, 30,* 87–90.

Springer, G., Schachner-Korn, D., & Long, J. V. P. (1964). Metastable solid dilution reactions in the system FeS2-CoS2-NiS2. *Economic Geology, 59,* 475–491.

Sylvester, P. (2008). Laser ablation ICP-MS in the earth sciences: Current practices and outstanding issues. In: *Mineralogical Association of Canada.* Short Course **40**, p 356.

Tornos, F. (2006). Enviroment of formation and styles of volcanogenic massive sulfides. The Iberian Pyrite Belt. *Ore Geology Reviews, 28,* 259–307.

Tornos, F., & Conde, C. (2002). La influencia biogénica en la formación de los yacimientos de sulfuros masivos de la Faja Pirítica Ibérica. *Geogaceta, 32,* 235–238.

Tornos, F., González Clavijo, E., & Spiro, B. (1998). The Filón Norte orebody (Tharsis, Iberian Pyrite Belt): a proximal low-temperature shale-hosted massive sulphide in a thin-skinned tectonic belt. *Mineralium Deposita, 33,* 150–169.

Tornos, F., Solomon, M., Conde, C., & Spiro, B. F. (2008). Formation of the Tharsis massive sulfide deposit, Iberian Pyrite Belt: Geological, Lithogeochemical, and Stable Isotope Evidence for Deposition in a Brine Pool. *Economic Geology, 103,* 185–214.

Walshe, J. L., & Solomon, M. (1981). An investigation into the environment of formation of the volcanic-hosted Mount Lyell copper deposits using geology, mineralogy, stable isotopes and a six-component chlorite solid solution model. *Economic Geology, 76,* 246–284.

Yamaguchi, K. E., & Ohmoto, H. (2006). Evidence from sulfur isotope and trace elements in pyrites for their multiple post-depositional processes in uranium ores at the Stanleigh Mine, Elliot Lake, Ontario, Canada. *Geological Society of America Memoir, 2006,* 143–156.

Zhao, H. X., Frimel, H. E., Jiang, S. Y., & Dai, B. Z. (2011). LA-ICP-MS trace element analysis of pyrite from the Xiaoqinling gold district, China: Implications for ore genesis. *Ore Geology Reviews, 43,* 142–153.